Pure Appl. Chem., Vol. 76, No. 2, pp. 389–413, 2004.
© 2004 IUPAC

INTERNATIONAL UNION OF PURE AND APPLIED CHEMISTRY

MACROMOLECULAR DIVISION*

RHEOLOGICAL AND MECHANICAL PROPERTIES OF POLY(α-METHYLSTYRENE-*co*-ACRYLONITRILE)/ POLY(METHYLACRYLATE-*co*-METHYL METHACRYLATE) BLENDS IN MISCIBLE AND PHASE-SEPARATED REGIMES OF VARIOUS MORPHOLOGIES

PART IV. INFLUENCE OF THE MORPHOLOGY ON THE MECHANICAL PROPERTIES

(IUPAC Technical Report)

Prepared for publication by
V. ALTSTÄDT[1,‡], L. DE LUCCA FREITAS[1,†], AND D. W. SCHUBERT[2,**]

[1]*Department of Polymer Engineering, Technical University Hamburg-Harburg, D-21073 Hamburg, Germany;* [2]*GKSS Research Centre, Max-Planck-Strasse, D-21502 Geesthacht, Germany*

*Contributing Members of the Working Party for this report were as follows: V. Altstädt, D. W. Schubert, G. H. Michler, F. Ramsteiner (Germany), B. Pukánszky (Hungary), L. Glas (Belgium), J. P. Williams, D. R. Moore (UK).

‡Corresponding author; present address: Lehrstuhl für Polymere Werkstoffe, Universität Bayreuth, Universitätsstrasse 30, 95447 Bayreuth, Germany
†Permanent address: Instituto de Química, Universidade Federal do Rio Grande do Sul, Av. Bento Gonçalves, 9500, 91501-970 Porto Alegre, Brazil
**Present address: Freudenberg Forschungsdienst KG, Höherweg 2-4, 69465 Weinheim, Germany

Republication or reproduction of this report or its storage and/or dissemination by electronic means is permitted without the need for formal IUPAC permission on condition that an acknowledgment, with full reference to the source, along with use of the copyright symbol ©, the name IUPAC, and the year of publication, are prominently visible. Publication of a translation into another language is subject to the additional condition of prior approval from the relevant IUPAC National Adhering Organization.

Rheological and mechanical properties of poly(α-methylstyrene-*co*-acrylonitrile)/ poly(methylacrylate-*co*-methyl methacrylate) blends in miscible and phase-separated regimes of various morphologies

Part IV. Influence of the morphology on the mechanical properties

(IUPAC Technical Report)

Abstract: Influences of the morphology on the thermal and mechanical properties of poly(α-methylstyrene-*co*-acrylonitrile)/poly(methylacrylate-*co*-methyl methacrylate) (PαMSAN/PMMA) blends have been investigated. Differential scanning calorimetry (DSC) measurements confirm that all blends were phase-separated due to the temperature at which they have been extruded and squeeze-molded. Based on the cloudpoints of 17 blends and transmission electron microscopy (TEM) micrographs, the interaction parameters as a function of temperature and composition were calculated for the lower critical solution temperature (LCST) system. Varying the morphology by annealing without changing the composition of the system resulted in a finer morphology for the 85/15 blends, while the 40/60 blend showed an increase in the domain size with annealing time. Tensile strength and fracture toughness indicate that the PαMSAN domains in the tougher PMMA matrix cause a deterioration in the mechanical properties of the blends, while the PMMA domains in the PαMSAN matrix improve the mechanical properties. No clear conclusions on the influence of morphology on fracture toughness could be drawn because in one case (40/60 blend) the fracture toughness decreases slightly by annealing and in the other case (85/15 blend) fracture toughness values increase slightly with decreasing phase separation by annealing. In situ strained thin sections in the TEM indicated no effect of annealing on the micromechanical behavior. Shear deformation was observed as the prevailing deformation mechanism in the PαMSAN and fibrillized crazing in the PMMA-rich blends. From fatigue crack growth experiments it was concluded that the fatigue crack propagation threshold is higher for PMMA than for PαMSAN. Tests on the annealed samples of PαMSAN/PMMA 85/15 and 40/60 showed that the differences in morphology did not affect the fatigue crack growth resistance significantly. From the features of the fracture surface investigated by scanning electron microscopy (SEM), the conclusion can be drawn that the fatigue crack propagates faster in the more brittle PαMSAN phase, but the overall advance of the crack front is controlled at the interphases, resulting in a crack propagation gradient along the interphase.

LIST OF CONTRIBUTORS

Laboratory number	Representative	Institution
[1]	V. Altstädt	Until 1995: BASF, Ludwigshafen, Germany; 1995–2000: TU Hamburg-Harburg, Hamburg, Germany; Since 2000: University Bayreuth, Bayreuth, Germany
[2]	L. Glas	Shell, Ottignies Lovain la Neuve, Belgium
[3]	B. Pukánszky	TU Budapest, Budapest, Hungary
[4]	D. W. Schubert	GKSS, Geesthacht, Germany
[5]	G. H. Michler J. Laatsch	University Halle-Wittenberg, Merseburg, Germany
[6]	R. Moore	ICI Technology, Middlesbrough Cleveland, England
[7]	J. G. Williams	Imperial College, London, UK
[8]	F. Ramsteiner	BASF, Ludwigshafen, Germany

HISTORIC BACKGROUND

The former Working Party chairman H. H. Meyer at the Cranfield meeting in 1988 initiated a collaborative feasibility study on "Polymer Mixtures with Non-bonding and Bonding Interactions" within IUPAC Working Party IV.2.1. L. A. Utracki further developed the concept of polymer mixtures with non-bonding interactions. He proposed a program on immiscible/miscible blends for the components PαMSAN and PMMA. Both are amorphous polymers that are relatively stable in the molten state. For this system, blends with controlled morphology can be prepared, i.e., single-phase blends below the lower critical solution temperature (LCST) and phase-separated blends at temperatures above it.

BASF Aktiengesellschaft provided samples of PαMSAN and PMMA with similar viscosity functions at 210 °C. In a former paper, the characterization of the constituents, the preparation and annealing of the blends and an overview of blend morphology has been presented [1]. In a paper by V. Schytt and J. Lyngaae-Jørgensen [2], the limits of miscibility in the quiescent state and during flow has been discussed. I. Vinckier and H. M. Laun reported the manifestation of the interface in oscillatory shear measurements [3,4], and Z. I. Zang, Y. L. Yang, I. Vinckier, and H. M. Laun compared, measured, and simulated morphologies under oscillatory shear [5]. D. W. Schubert investigated the χ-parameter and the phase diagram of PαMSAN/PMMA blends by cloudpoint and neutron-scattering techniques [6].

OBJECTIVE

The joint project aims at the preparation of blends of PαMSAN and PMMA and the investigation of their rheological and mechanical properties. An especially interesting feature of these blends is the possibility of strongly influencing the morphology without changing the composition. For a given blend composition, miscible and immiscible blends with different domain sizes can be obtained by annealing the system at different temperatures and periods of time.

Blends with different compositions and blends with the same composition, but different morphologies have been prepared. Data about polymer characterization, blend preparation, and morphology have already been published [1]. Also, the influence of blend composition and morphology on the rheological properties of the blends was investigated [1–5].

In this paper, we present a detailed investigation of the mechanical properties of these blends. Blends with four different compositions have been prepared, and two of the blends have been annealed under different conditions in order to investigate the influence of morphology on the mechanical properties. The following properties have been investigated:

- tensile properties
- fracture toughness
- fatigue crack propagation resistance

Furthermore, the phase diagram and the thermal and thermo-mechanical properties of the blends as a function of blend composition and morphology are discussed.

RELATED LITERATURE

Most commercially important polymer pairs are immiscible, and the properties of the resulting materials depend on several factors like chemical structure and molecular weight of the polymers and also on the processing conditions. Extensive literature about this subject has been published [7–11]. One of the main factors that influence the mechanical properties, reliability, and function of the final material is the strength of interfaces between the phase domains [11]. The strength of the interface depends on the structure and connectivity of the phases. The evolution of structure at the interface is controlled by the dynamics of the chains and the thermodynamics of the interacting species. At an incompatible polymer interface, monomer units from one side diffuse to the other side until an equilibrium distribution is reached having a characteristic interfacial width. The greater the amount of mixing or chain interpenetration at the interface, the greater the improvement in strength.

The miscibility of PαMSAN/PMMA blends has been investigated [1,2,7], as well as the influence of composition and morphology on the rheological properties of these blends [3–6].

Willet and Wool [12] investigated the influence of the acrylonitrile content on the strength of PSAN/PMMA interfaces. The blend of PMMA with PSAN containing a mass fraction of 23 % AN was miscible, while the blends with PSAN containing mass fractions of 5.7 and 37 % were immiscible. Annealing apparently did not affect the miscibility of these systems. These results were in agreement with the ones obtained by Fowler, Barlow, and Paul [13]. X-ray photoelectron spectroscopy (XPS) analysis of the fracture surfaces after welding at 125 °C showed a cohesive fracture for the blends of PMMA with PSAN containing a mass fraction of 5.7 and 23 % AN and a combination of cohesive and adhesive failure for the system with a mass fraction of 37 % AN [12]. The fracture surfaces were also investigated by SEM. The fracture surfaces of the PSAN/PMMA interfaces with a mass fraction of 5.7 % showed matching parallel lines 10–20 μm apart, aligned perpendicular to the crack propagation direction. The miscible PSAN/PMMA blend with a mass fraction of 23 % AN showed a similar pattern, but with a distance between the lines of about 10 μm. The analysis of the surfaces of the PSAN/PMMA interfaces with a mass fraction of 37 % AN indicated a quite discontinuous crack growth, snapping rapidly for several hundred micrometers, then growing slowly for a time before snapping again (banded structure) [12].

EXPERIMENTAL

Materials

The materials used for the investigation were commercially available copolymers manufactured by BASF. Luran KR 2556 is a copolymer of α-methylstyrene and acrylonitrile, PαMSAN, with a mass fraction of 30 % acrylonitrile (M_w = 82 000 g/mol; M_w/M_n = 2.3) [2] and Lucryl G77 is a poly(methyl methacrylate), PMMA, with a mass fraction of 5 % methyl acrylate (M_w = 88 000 g/mol; M_w/M_n = 2.0) [2]. The chemical structure of the polymers is shown in Fig. 1.

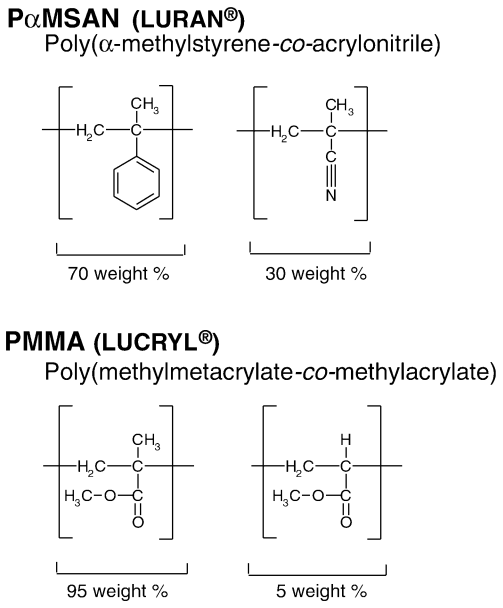

Fig. 1 Chemical structures of PαMSAN and PMMA.

Blend preparation

The pellets of neat PαMSAN and PMMA were blended in a double-cone blender. The dry pellet mixtures (including the mixtures 0/100 and 100/0) were fed from a single-screw volumetric feeder to a ZSK30/2 twin-screw extruder at 212 °C/200 °C. An overview of blend composition and nomenclature is given in Table 1.

Table 1 Nomenclature, composition, and annealing conditions of the PαMSAN/PMMA blends.

Polymer blend	*w*(PαMSAN)/%	Annealing conditions			
PαMSAN/PMMA 85/15	85	none	1 h/195 °C	4 h/180 °C	24 h/170 °C
PαMSAN/PMMA 60/40	60	none			
PαMSAN/PMMA 40/60	40	none	1 h/195 °C	4 h/195 °C	4 h/220 °C
PαMSAN/PMMA 15/85	15	none			

Sample preparation

Sample plaques for distribution to the participants were obtained in a two-step process by squeeze-molding. In the first step, the pellets were filled in a frame ($180 \times 180 \times 4$ mm) and pressed with an electrically heated press at 230 °C and 5 bar for 7 min. The preconsolidated sample was immediately moved to a steam press, preheated to 195 °C. The final consolidation was then done at 195 °C and 80 bar for 4 min. Cooling to room temperature proceeded within 70 s under 80 bar pressure.

Annealing

In order to investigate the influence of morphology on the properties of the PαMSAN/PMMA blends, some of the blends were annealed for different times at different temperatures. Firstly, the samples were cut to a size of $170 \times 170 \times 3.7$ mm. A steel frame of the same size was used during annealing to keep

the plaques in shape. In order to prevent bubble formation, a small pressure has been applied to the samples during annealing. Each sample was annealed separately and slowly cooled down to room temperature. An overview of the annealing conditions of the samples is given in Table 1.

Cloudpoint curve

Laboratory 4 has determined the cloudpoint curve. The polymers were dissolved in acetone and mixed in the appropriated composition (typically, 300 mg of the polymers were used). The solution was dropped with a Pasteur pipette onto a glass plate at 50 °C. The samples were dried further at 50 °C at reduced pressure in an oven for 3 days. Afterwards, the samples were annealed at the desired temperature and reduced pressure in an oven for several days, and the presence or absence of cloudness was visually observed.

Transmission electron microscopy (TEM)

Laboratories 1 and 5 investigated the morphology of the blends by TEM. In both laboratories, ultra-thin cuts of the samples were prepared. The cuts were then treated with RuO_4 in order to obtain enough contrast between the phases. In these blends, RuO_4 reacts selectively with PαMSAN.

Light microscopy

Laboratory 1 investigated the influence of annealing on the morphology of the PαMSAN/PMMA 40/60 blend by light microscopy. Thin cuts of the samples (10–50 μm) were obtained, but have not been stained. The microscopic investigations were carried out in transmission.

Differential scanning calorimetry

Laboratory 2 determined the glass-transition temperatures of the blends by differential scanning calorimetry (DSC), using a Perkin-Elmer DSC 7. Small pieces of the delivered plaques were crushed with a hammer and weighed in the DSC crucibles. The experiments were carried out at a heating rate of 10 °C/min.

Dynamic mechanical analysis

Dynamic mechanical analysis was performed in torsion in a Rheometrics Dynamical Analyser (RDA II) at a frequency of 1 Hz at Laboratory 1. The temperature was varied stepwise between –50 and 150 °C (–50 to 80 °C: data points each 3 °C; 80 to 150 °C: data points each 1 °C).

Laboratory 2 used dynamic mechanical analysis to investigate the region of the α-relaxation of the PαMSAN/PMMA 85/15 blend. The test was performed in torsion at a frequency of 1 Hz and with a heating rate of 1 °C/min using an RDA II from Rheometrics.

Tensile and flexural properties

Laboratory 3 has determined the tensile strength and the elongation at break with standard ISO dog-bone specimens cut from the delivered plaques. The measurements were carried out with a Zwick 1445 mechanical testing machine using a cross-head speed of 5 mm/min. Five specimens of each sample have been tested. For the determination of Young's modulus, tests with standard ISO dog-bone specimens were performed at 0.5 mm/min in an FPZ 10 universal mechanical testing machine (Fritz Heckert, Germany). Also, in this case five specimens of each sample have been tested.

The flexural tests were performed with specimens of dimensions 80 × 10 × 4 mm in a FPZ 10 universal mechanical testing machine. The distance between the supports was 60 mm, and the crosshead speed 2 mm/min.

Micromechanics

Laboratory 5 investigated the micromechanical deformation of the PαMSAN/PMMA blends. Thin sections of the samples were cut with a microtome. The sections were about 0.5 μm thick, 0.5 mm wide, and 3 mm long. Each section was fixed between two adhesive tapes. These adhesive tapes are suitable for work under vacuum and were supplied with a 1-mm hole in the middle of each. The sample was fixed across these holes. Afterwards, the tapes were put into the tensile device of the microscope and the parts of the tapes beside the holes were cut out. The microscopic investigation was carried out on a high-voltage electron microscope (1000-kV-TEM, Max Planck Institute of Microstructure Physics, Halle/S., Germany).

Fracture toughness

Fracture toughness tests have been performed together by Laboratories 1 and 8. Compact tension (CT) specimens with dimensions 62.5 × 60 mm were cut from the plaques, and the notches were introduced via a milling machine. A crack was subsequently introduced by razor tapping. Fracture tests were conducted on a Zwick 1485 machine with a rate of 10 mm/min at room temperature (about 23 °C). The force was measured with a 5 kN load cell and the crack opening displacement (COD) with a COD gauge (MTS model 632.11C-23) mounted in front of the specimen. The calculations were carried out according to a calibration function given in ASTM E 399-83. An LEFM analysis to determine K_{IC} was carried out according to an ISO protocol [14].

Fatigue crack propagation

The fatigue crack propagation tests were carried out with compact tension specimens (CT-specimens) at room temperature by Laboratory 1, in accordance with an ISO protocol [15]. Specimens with dimensions 62.5 × 60 mm were cut from the plaques, and a natural pre-crack was introduced. The tests were conducted on a MTS 300.05 servo-hydraulic test machine at a frequency of 10 Hz and a stress ratio $R = 0.1$. The COD was measured using a COD gauge mounted in front of the specimen. After the tests, the fracture surface morphology was investigated by using SEM.

Scanning electron microscopy (SEM)

The crack surfaces of the CT-specimens (fatigue crack propagation experiments) were investigated by SEM (Laboratory 1). The samples were attached to the sample holder with a conducting graphite adhesive. A 15-nm gold layer was sputtered on the samples. The micrographs were taken at an angle between 10° and 30° in order to observe the surface relief.

RESULTS

Phase diagram and morphology of the blends

The influence of annealing on the blend morphology and, consequently, on properties can only be understood with knowledge of the phase diagram for a specific system. The PαMSAN/PMMA blends have an LCST at about 160 °C. The exact position of the LCST depends on the composition and molecular weight of both copolymers. In a former paper, V. Schytt and J. Lyngaae-Jørgensen [2] deter-

mined the point curve of the PαMSAN/PMMA blends using laser light-scattering. The measurements indicated an LCST of 157 °C and a nonsymmetric phase diagram with an LCST for the PαMSAN-rich phase than for the PMMA-rich phase. This result was in disagreement with data published by Laun on the basis of annealing and TEM measurements [1], where it was observed that PαMSAN-rich blends phase separate at higher temperatures than PMMA-rich blends. However, V. Schytt and J. Lyngaae-Jørgensen [2] also observed that for the PαMSAN-rich blend (a mass fraction of 15 % PMMA) there were two cloudpoints with a zone of larger transparency between them and that the "true" binodal could be at the second cloudpoint at about 195 °C. The authors also considered the reproducibility of cloudpoints between mass fractions of 10 and 40 % PMMA being poor. For samples with higher PMMA contents, the cloudpoints and the binodal curve coincide.

Additional investigations on the phase diagram of the PαMSAN/PMMA blends have been performed by Laboratory 4 while Laboratories 1 and 5 investigated the morphology of the blends by TEM.

For the construction of the phase diagram, the cloudpoint of 17 blends with different compositions varying between mass fractions of 5 and 80 % PαMSAN were determined (Fig. 2). It has been reported recently that the interaction parameter for PαMSAN/PMMA blends depends on temperature and composition [6]. For the calculation of the interaction parameter, an equation with three adjustable parameters was used:

$$\chi = (A + B/T)[1/(1 + \alpha\phi)]$$

where χ = interaction parameter; A, B, α = adjustable parameters; T = temperature in K; and ϕ = volume fraction of PαMSAN.

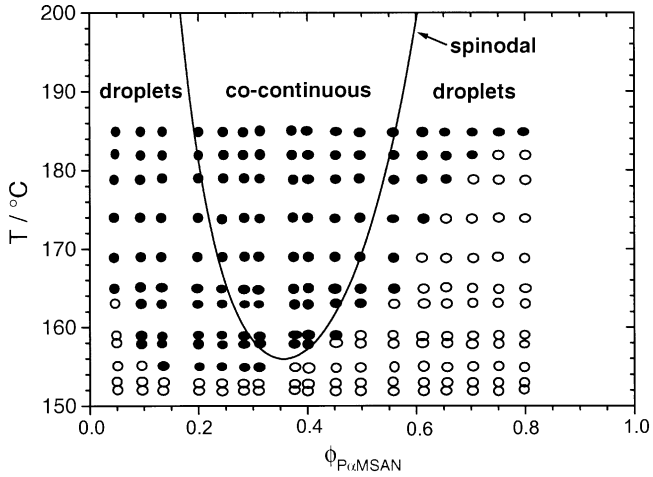

Fig. 2 Phase diagram of the PαMSAN/PMMA blends: o clear samples; ● cloudy samples; curve: calculated spinodal.

Therefore, three spinodal points must be obtained experimentally in order to determine the parameters. These points can be obtained from the cloudpoint diagram (Fig. 2) and the TEM micrographs (Fig. 3). In the micrographs, the PαMSAN-rich phase appears dark while the white phase is the PMMA-rich phase.

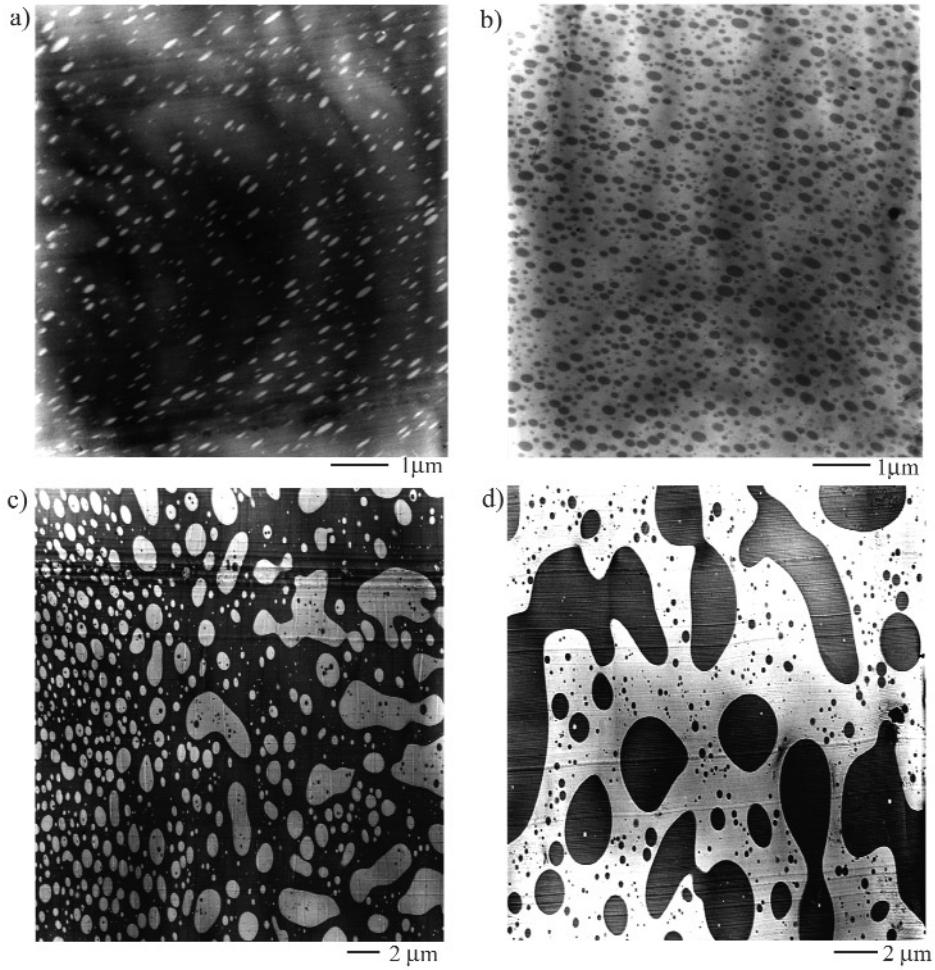

Fig. 3 TEM micrographs of PαMSAN/PMMA blends at different compositions: (a) 85/15; (b) 15/85; (c) 60/40; (d) 40/60.

With respect to the cloudpoint curve, the minimum must be in the range between 20 and 35 % PαMSAN (see Fig. 2). In the TEM micrograph of the blend PαMSAN/PMMA 15/85 (Fig. 3b) at 200 °C (the temperature at which the blend has been prepared), a droplet morphology is obtained and therefore the spinodal must be on the right-hand side of that point. This forces the parameter a to be close to 0.4—thus, $a = 0.4$ has been used for the calculation of χ. A further condition is the minimum temperature of the cloudpoint curve, which must be also very close to the minimum temperature of the spinodal (see Fig. 2) [6]. The third condition was obtained from the TEM micrograph of the PαMSAN/PMMA 60/40 blend at 200 °C (Fig. 3c). In this micrograph, both a droplet and a co-continuous morphology can be observed; it has been assumed that this mixed morphology resulted from slight temperature differences within the sample. Nevertheless, the spinodal, that represents the boundary line for these two morphologies, must be very close to 200 °C for the PαMSAN/PMMA 60/40 blend.

Finally, the interaction parameter was calculated using the equation:

$$\chi = (0.009533 - 3.09/T)[1/(1 + 0.4\phi)]$$

and was used to calculate the spinodal curve shown in Fig. 2.

The morphologies of the PαMSAN/PMMA 40/60 and PαMSAN/PMMA 85/15 blends at 200 °C are also consistent with the calculated spinodal.

Furthermore, the morphology of the annealed PαMSAN/PMMA 85/15 and PαMSAN/PMMA 40/60 blends was investigated. In Fig. 4, the TEM micrograph of the PαMSAN/PMMA 85/15 blend after annealing at 170 °C for 24 h is shown. After annealing, much fewer PMMA domains can be observed compared with the unannealed sample (Fig. 3a), indicating that the PMMA phase dissolved in the PαMSAN matrix. This result is in agreement with the optical observation that the transparency of the sample increases after annealing [16] and with the phase diagram described above. The PαMSAN/PMMA 85/15 blend is in the miscible regime at 170 °C, and actually a one-phase system would be expected after annealing. The presence of PMMA domains indicates that the dissolution of the PMMA domains is a slow diffusion-controlled process and was yet not complete, even after 24 h.

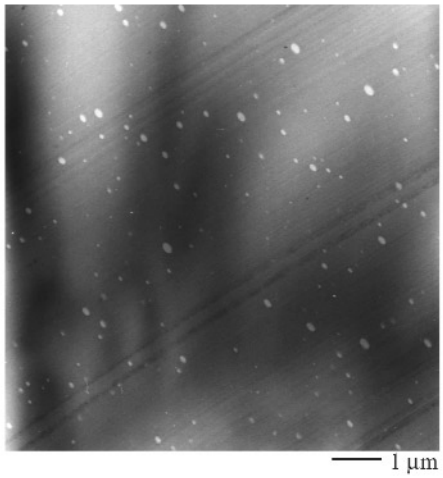

Fig. 4 TEM micrograph of the PαMSAN/PMMA 85/15 blend annealed at 170 °C for 24 h.

Figure 5 shows the histograms of the particle diameter distribution normalized to the number of particles for the unannealed and annealed PαMSAN/PMMA 85/15 blends. The particle diameter seems

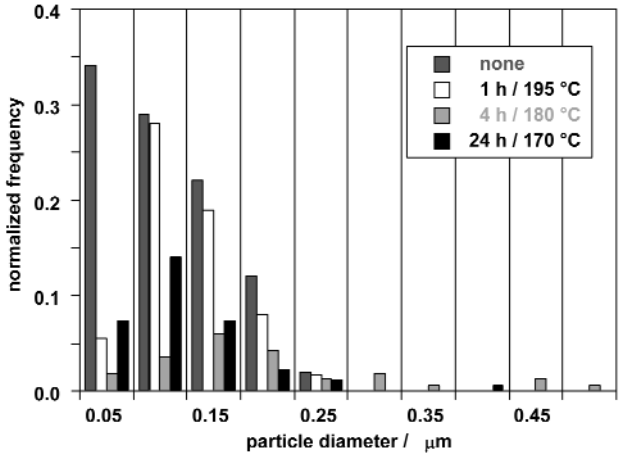

Fig. 5 Histograms of the particle diameter distribution normalized to the number of particles for the PαMSAN/PMMA 85/15 blends with different annealing conditions.

to increase after annealing, but the number of particles decreases drastically, especially for the samples annealed at 180 and 170 °C.

In Laboratory 1, the effect of annealing on the morphology of the PαMSAN/PMMA 40/60 blend was investigated by light microscopy. Light microscopy gives a better idea of the development of the phase morphology with annealing for this particular blend composition. In Fig. 6, the light micrographs of the unannealed and annealed PαMSAN/PMMA 40/60 blends are shown. The unannealed sample presents the finer co-continuous phase distribution. For the samples annealed for 1 h and 4 h at 195 °C and for 4 h at 220 °C, a coarser morphology can be observed. The domain size increases with annealing time and/or temperature. Consequently, the blend annealed for 4 h at 220 °C presents the coarsest morphology.

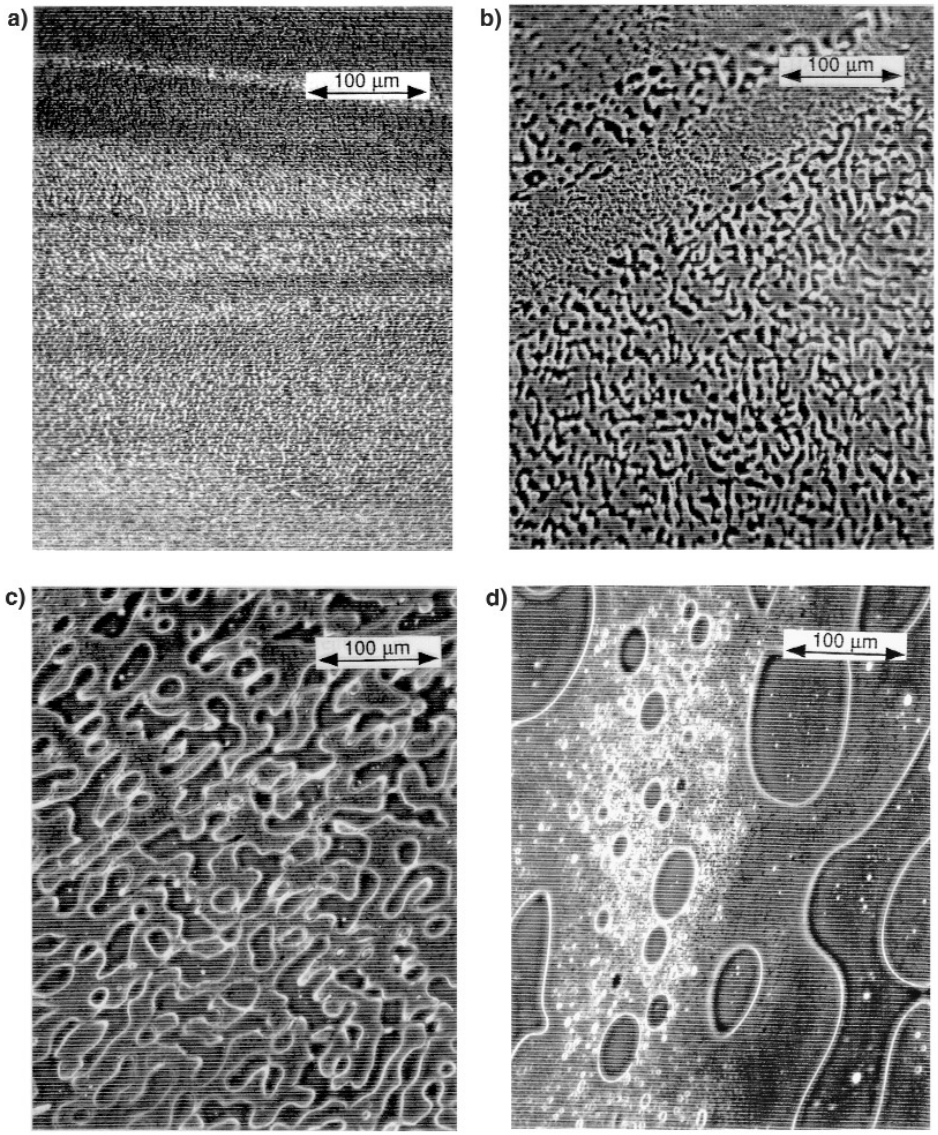

Fig. 6 Light micrographs of the PαMSAN/PMMA 40/60 blend unannealed (a) and annealed: 1 h/195 °C (b); 4 h/195 °C (c); and 4 h/220 °C (d).

Differential scanning calorimetry

The glass-transition temperatures, T_g, of the pure components and the blends were determined by Laboratory 1 using DSC. The glass-transition temperature of the PαMSAN sample is 119.6 °C and for PMMA copolymer is 109.4 °C (Table 2; Fig. 7). The derivative curve (Fig. 7b) shows clearly the broadening of the DSC curve at lower temperatures, in the region where the T_g of PMMA should be observed. For the blend of PαMSAN/PMMA 85/15 only one glass-transition temperature could be detected by DSC (Fig. 7), even though transmission electron micrographs show the presence of two phases (Fig. 3a). For the PαMSAN/PMMA blends with composition 60/40, 40/60, and 15/85, two T_gs can be observed (Table 2; Fig. 7). The glass-transition temperatures of the components in the blends are about the same as the T_gs determined for the neat components (Table 2), indicating immiscibility of the components.

Table 2 Glass-transition temperatures of the pure components and the blends determined by DSC at a heating rate of 10 °C/min.

w(PαMSAN)/ *w*(PMMA)	T_g(PαMSAN)/°C	T_g(PMMA)/°C	Annealing conditions
100/0	119.6	–	none
0/100	–	109.4	none
85/15	118.9		none
85/15	118.5		1 h/195 °C
85/15	118.4		4 h/180 °C
85/15	118.5		24 h/170 °C
60/40	120.5	109.4	none
40/60	120.9	108.0	none
40/60	120.0	107.8	1 h/195 °C
40/60	120.1	107.8	4 h/195 °C
40/60	120.0	107.0	4 h/220 °C
15/85	122.0	108.8	none

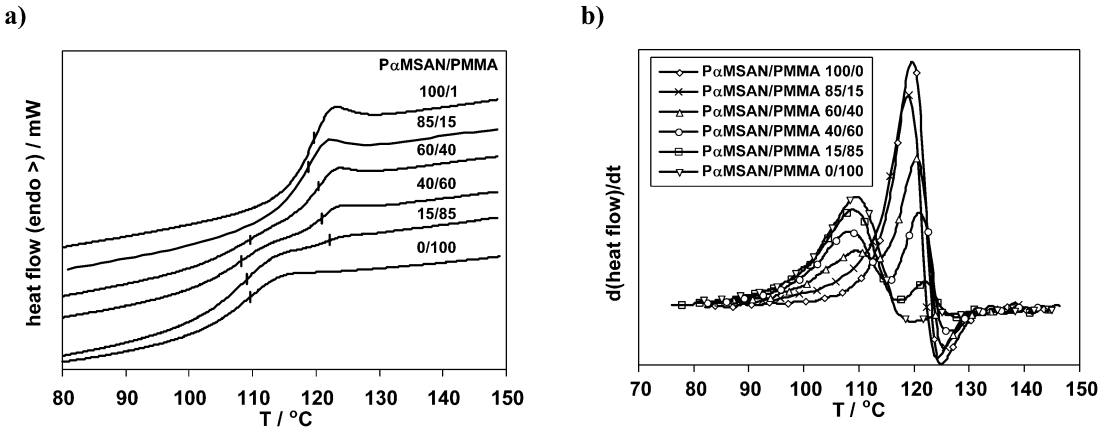

Fig. 7 DSC thermograms of PαMSAN/PMMA blends with different compositions; (a) integral curves; (b) derivative curves.

The glass-transition temperatures of the annealed PαMSAN/PMMA blends have also been determined. Although differences in the morphology have been observed by microscopy, no significant changes in the glass-transition temperatures of the phases could be observed (Fig. 8). After annealing,

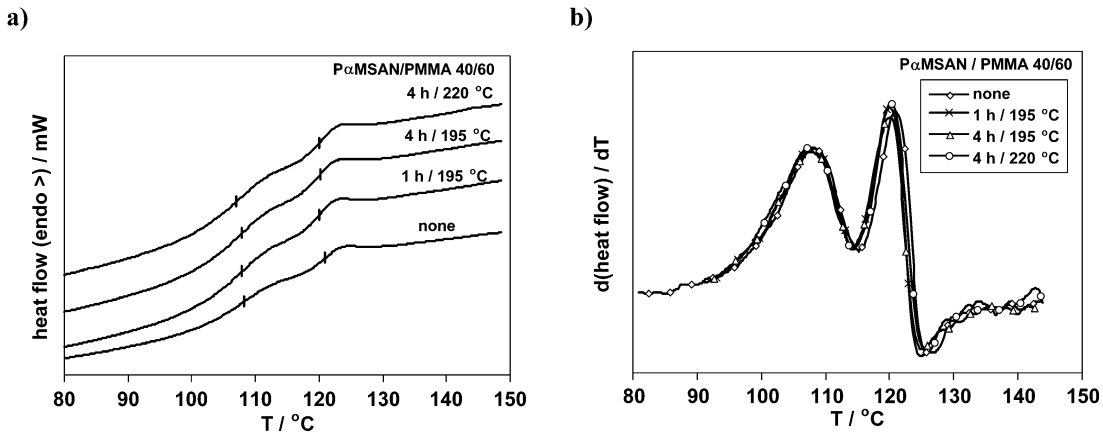

Fig. 8 DSC thermograms of the PαMSAN/PMMA 40/60 blend after annealing under different conditions; (a) integral curves; (b) derivative curves.

the number of PMMA domains decreases for the blend with a mass fraction of 85 % PαMSAN (Fig. 4) and again only one T_g was observed (Table 2) for this blend composition.

Dynamic mechanical analysis

Dynamic mechanical analysis was carried out by Laboratory 1. Figure 9 shows the storage and the loss moduli for PαMSAN and PMMA. The storage modulus of PαMSAN is almost constant for temperatures lower than 60 °C. Its loss modulus presents only one peak with a maximum at 123 °C. This peak corresponds to the α-relaxation or glass transition of the polymer. It is also important to notice that the α-relaxation of this sample is very broad. The behavior of the PMMA is more complex. The loss modulus curve shows a strong peak with a maximum at 109 °C that corresponds to the α-relaxation or glass transition of the polymer. In the same curve, a very broad peak centered at 8 °C can also be observed. This peak corresponds to the β-relaxation of PMMA and is attributed to the rotation of the -$COOCH_3$ side groups [17]. This relaxation influences also the storage modulus of PMMA, which increases slightly below the glass-transition temperature.

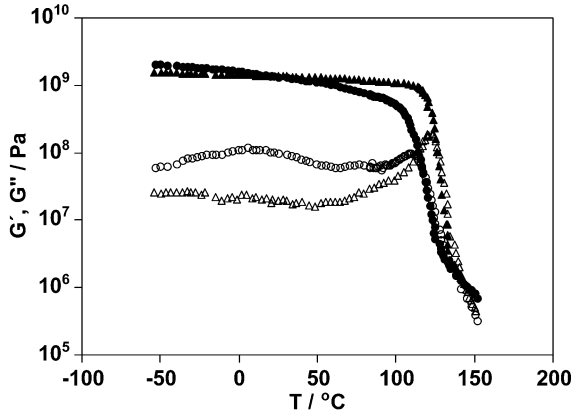

Fig. 9 Logarithm of the storage and loss modulus as a function of temperature for PαMSAN (▲, Δ) and PMMA (●, ○). (ν = 1 Hz)

Figure 10 shows the storage modulus and the tan δ curves for PαMSAN, PMMA, and their blends in the temperature range of the α-relaxation. The tan δ curve of PMMA (Fig. 10b) shows a very broad peak with a maximum at 124 °C. The maximum for the PαMSAN curve is located at 132 °C. The behavior of the PαMSAN/PMMA 15/85 blend is dominated by the PMMA matrix (see Fig. 3b), while the behavior of PαMSAN/PMMA 85/15 blend is dominated by the PαMSAN. In both cases, only one maximum can be observed in this temperature range, though two phases are present in the blends (see Fig. 3). For the PαMSAN/PMMA 40/60 and PαMSAN/PMMA 60/40 blends quite a different behavior can be observed. In both cases, the peak maximum is located at about 131 °C, but a distinct shoulder is observed at lower temperatures. The intensity of this shoulder increases with increasing PMMA content and was attributed to the α-relaxation of PMMA. The fact that the glass-transition temperatures of PαMSAN and PMMA are less than 20 °C apart and that the α-relaxation of the PαMSAN sample is very broad can explain the difficulty of identifying two separated relaxation processes in the blends, even though they are phase-separated.

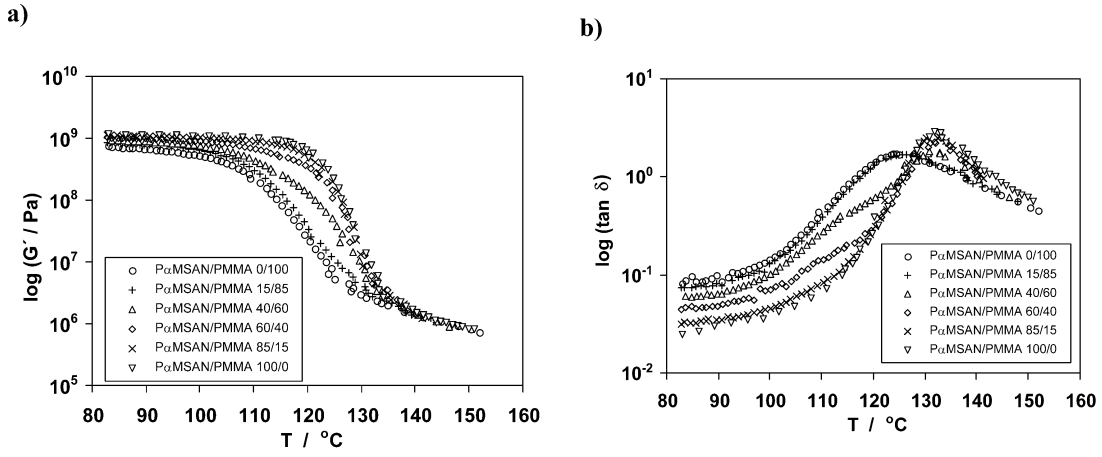

Fig. 10 Logarithm of the storage modulus and of tan δ as a function of temperature for PαMSAN, PMMA, and their blends. (ν = 1 Hz).

Tensile and flexural properties

Laboratory 3 investigated the tensile and flexural properties of the PαMSAN/PMMA blends. The results are presented in Table 3 and in Figs. 11–13.

Figure 11 shows Young's modulus as a function of the blend composition. PαMSAN has a higher modulus than PMMA. Young's moduli for the blends lie between the moduli of the neat components and increase linearly with increasing amount of PαMSAN in accordance with the rule of mixtures. For the flexural modulus a similar behavior has been observed (Fig. 11). The tensile strength and the elongation at break are lower for the blends with a PMMA matrix than for the blends with a PαMSAN matrix (Table 3; Figs. 12 and 13). A possible explanation for this behavior is that the presence of PαMSAN brittle domains in the PMMA matrix (less brittle) causes a deterioration in the mechanical properties of the blends, while the presence of the tougher PMMA domains in the PαMSAN matrix contributes to an improvement in their properties.

Also, the influence of the annealing conditions on the tensile and flexural properties of the blends PαMSAN/PMMA 85/15 and 40/60 has been investigated. In both cases, Young's moduli decrease after the samples have been annealed, but no clear dependence of their values on annealing conditions can be established (Table 3).

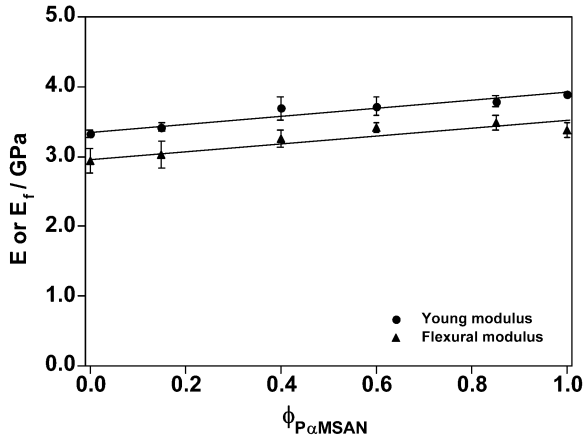

Fig. 11 Young's and flexural moduli of the blends as a function of the mass fraction of PαMSAN.

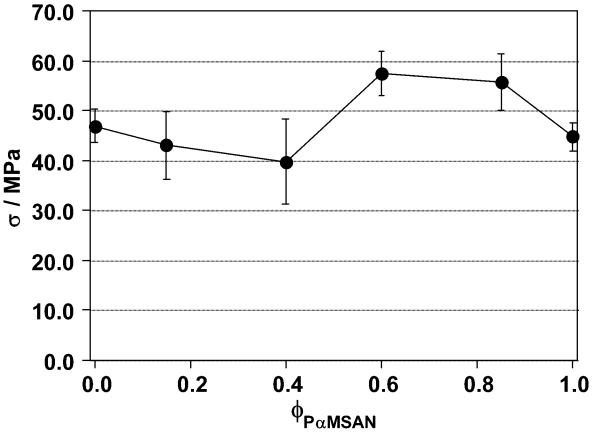

Fig. 12 Tensile strength of the blends as a function of the mass fraction of PαMSAN.

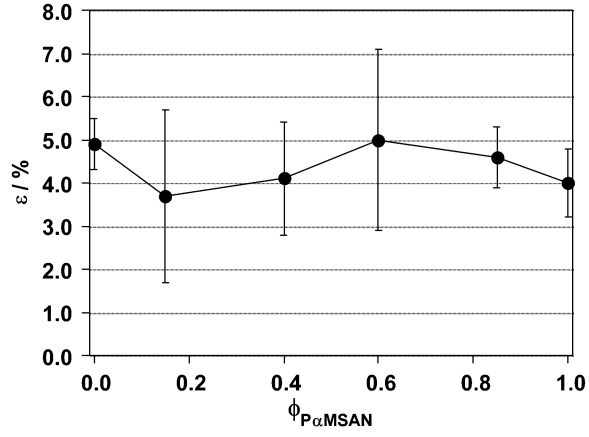

Fig. 13 Relative elongation at break of the blends as a function of the mass fraction of PαMSAN.

Table 3 Tensile and flexural properties of the PαMSAN/PMMA blends as a function of composition and annealing conditions.

w(PαMSAN)/ *w*(PMMA)	Annealing conditions	*E*/GPa	σ/MPa	ε/%	E_f/GPa	σ_f/MPa
100/0	none	3.89 ± 0.06	44.8 ± 2.8	4.0 ± 0.8	3.38 ± 0.10	77.8 ± 7.4
85/15	none	3.79 ± 0.06	55.7 ± 5.6	4.6 ± 0.7	3.49 ± 0.11	90.1 ± 10.6
85/15	1 h/195 °C	3.59 ± 0.06	34.3 ± 2.6	2.0 ± 0.2	3.46 ± 0.03	92.4 ± 4.5
85/15	4 h/180 °C	3.69 ± 0.07	55.2 ± 3.5	4.5 ± 0.6	3.52 ± 0.07	97.6 ± 3.1
85/15	24 h/170 °C	3.66 ± 0.04	51.2 ± 5.2	3.9 ± 0.6	3.59 ± 0.02	94.0 ± 10.0
60/40	none	3.72 ± 0.17	57.4 ± 4.4	5.0 ± 2.1	3.42 ± 0.07	93.4 ± 2.7
40/60	none	3.69 ± 0.13	39.8 ± 8.6	4.1 ± 1.3	3.26 ± 0.13	92.3 ± 4.4
40/60	1 h/195 °C	3.59 ± 0.06	52.0 ± 6.5	4.7 ± 1.8	3.14 ± 0.09	90.3 ± 2.8
40/60	4 h/195 °C	3.66 ± 0.06	51.9 ± 2.2	4.6 ± 0.8	3.20 ± 0.08	80.4 ± 4.8
40/60	4 h/220 °C	3.46 ± 0.11	48.6 ± 6.4	3.8 ± 0.8	3.27 ± 0.06	95.9 ± 2.9
15/85	none	3.42 ± 0.08	43.1 ± 6.8	3.7 ± 2.0	3.03 ± 0.19	84.7 ± 5.4
0/100	none	3.33 ± 0.04	46.9 ± 3.3	4.9 ± 0.6	2.94 ± 0.18	83.8 ± 4.6

Micromechanics

Investigation of the micromechanical deformation behavior was performed by Laboratory 5 on the following samples: unannealed and annealed PαMSAN/PMMA 85/15 blends and unannealed PαMSAN/PMMA 60/40 blend. Blends with higher PMMA contents were very sensitive to the highly energetic electron beam and could not be investigated.

Figure 14 shows micrographs of the unannealed PαMSAN/PMMA 85/15 blend under strain. The deformed structure resembles very much the one observed for neat PαMSAN. Shear deformation can be observed mainly due to the formation of homogeneous crazes and rhombus-like deformation zones as starting points for shear bands. Figure 14b shows the sample with a higher magnification, and it is

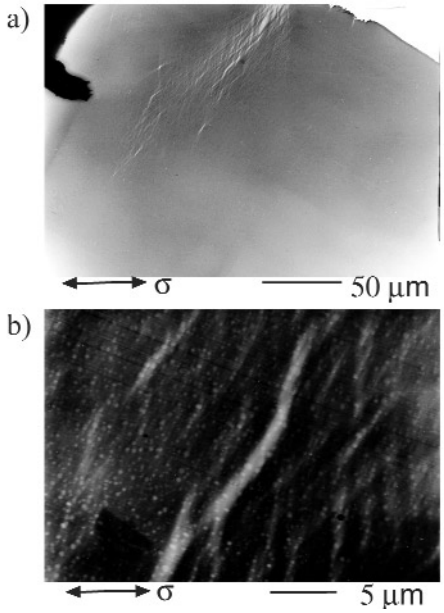

Fig. 14 In situ strained thin section of the unannealed PαMSAN/PMMA 85/15 blend (a) with low and (b) with higher magnification.

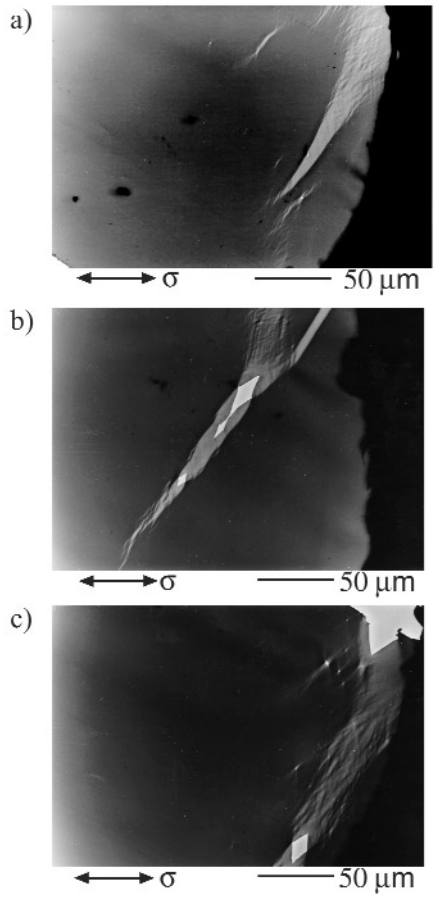

Fig. 15 Strained thin sections of the PαMSAN/PMMA 85/15 blends annealed at (a) 1 h / 195 °C, (b) 4 h/180 °C, and (c) 24 h/170 °C.

possible to observe that the PMMA particles are not influenced by the deformation process. The differences in brightness between PαMSAN and PMMA result from the depolymerization of PMMA by the electron beam. For the annealed samples, a similar behavior was observed, independent of the annealing conditions (Figs. 15 and 16). However, a more detailed investigation shows that the starting points for shear-band formation are in some cases the PMMA particles (Fig. 17).

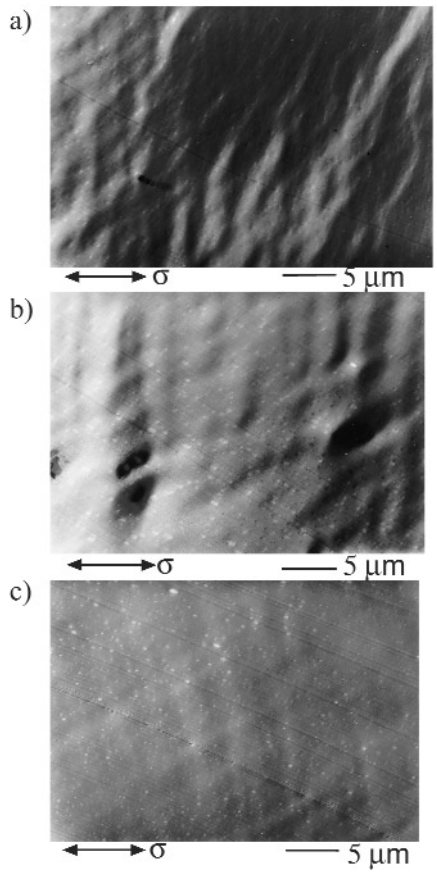

Fig. 16 Strained thin sections of the PαMSAN/PMMA 85/15 blends annealed at (a) 1 h/195 °C, (b) 4 h/180 °C, and (c) 24 h/170 °C with higher magnification.

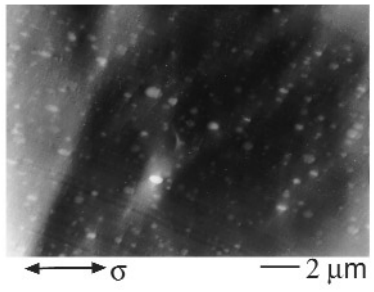

Fig. 17 Strained thin section of the PαMSAN/PMMA 85/15 blend annealed at 4 h/180 °C.

Figure 18 shows the micromechanical deformation structures of the PαMSAN/PMMA 60/40 sample. Fibrillized crazing followed by a cavitation process occurs in the PMMA phase. Although PαMSAN builds the matrix phase, the deformation behavior in this blend seems to be controlled by the dispersed PMMA phase.

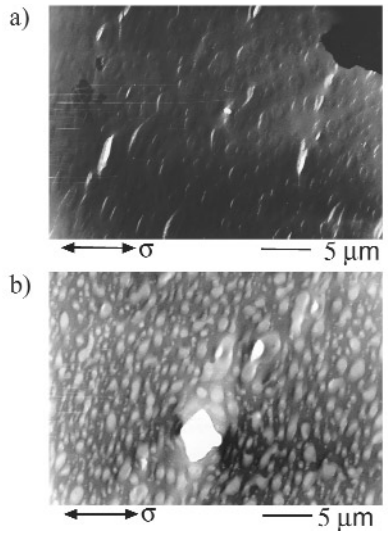

Fig. 18 Micromechanical deformation structure of an in situ strained thin section of the PαMSAN/PMMA 60/40 blend (a) fibrillized crazing occurs at the interphase between PαMSAN and PMMA phase, followed by cavitation of the whole PMMA particle (b) as a consequence of the homogeneous shear deformation in the PαMSAN matrix.

Fracture toughness

The fracture toughness measurements were jointly performed by Laboratories 1 and 8. The values of K_{IC} as a function of the blend composition are shown in Fig. 19. Neat PMMA exhibits markedly higher fracture toughness than neat PαMSAN. The K_{IC} values for all blends lie between the values of the neat components, but different tendencies can be observed, depending on which component the matrix is built. Firstly, the scattering of the K_{IC} values is much larger if PMMA builds the matrix. It seems, for example, that the addition of a mass fraction of 15 % PαMSAN to PMMA causes a remarkable drop of the K_{IC} value for this blend, but the drop is within the standard deviation of the data values. For the blends with a PαMSAN matrix, the scatter of the data is much smaller. It seems that the presence of PMMA domains in the PαMSAN matrix increases the fracture toughness of the blends and that the transition to higher fracture toughness lies between mass fractions of 40 and 60 % PαMSAN. That can readily be seen for the PαMSAN/PMMA 60/40 blend, which presents a markedly higher toughness than neat PαMSAN. A similar tendency was also observed for the ultimate tensile properties of the blends (see Figs. 12 and 13). Here, it seems that PαMSAN domains in the PMMA matrix act as defects

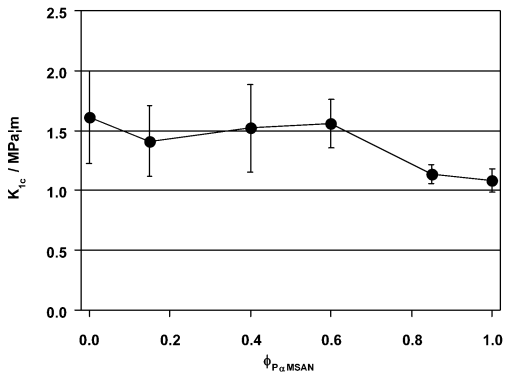

Fig. 19 K_{IC} values as a function of blend composition.

and cause a deterioration in the mechanical properties of the blends, while the tougher PMMA domains in the PαMSAN matrix contribute to an improvement in their properties.

Fracture toughness measurements have been also performed with the annealed samples. Figure 20 shows the K_{IC} values of the PαMSAN/PMMA 85/15 blend after annealing under different conditions. For the sample annealed for 1 h at 195 °C, a lower K_{IC} value than for the unannealed one was obtained. This can be attributed to degradation of the sample due to the high annealing temperature, since the annealed sample presented a more intensive yellow color than the unannealed one. For the samples annealed at lower temperatures, an increase in the K_{IC} values can be observed. In these cases, the predominant effect is probably the increase in the homogeneity of the blends after annealing, as can be observed in the TEM micrographs (Figs. 3a, 4, and 5).

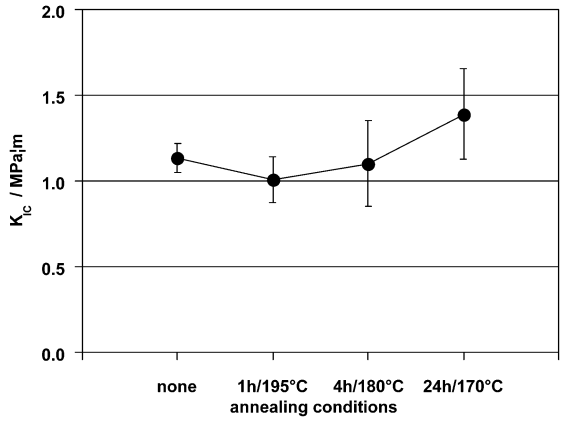

Fig. 20 K_{IC} values as a function of annealing conditions for PαMSAN/PMMA 85/15.

A different behavior has been observed for the annealed PαMSAN/PMMA 40/60 samples (Fig. 21). The K_{IC} values decrease with increasing annealing temperature and/or time. The micrographs of these blends show that, with increasing time and/or temperature, the domain sizes increase (Fig. 6). From these results, it can be concluded that the fracture toughness of the blends decreases with increasing phase separation.

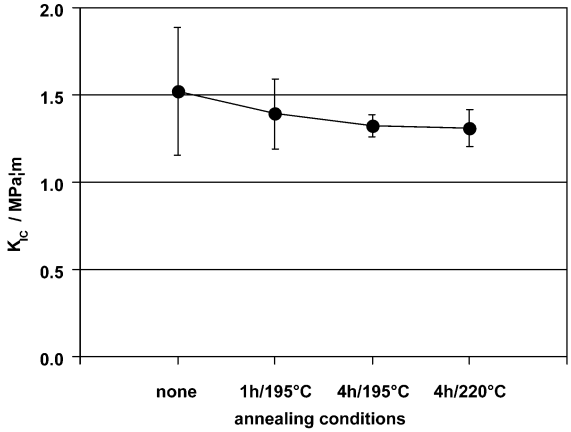

Fig. 21 K_{IC} values as a function of annealing conditions for PαMSAN/PMMA 40/60.

Fatigue crack propagation

A detailed study of the fatigue crack propagation has been published elsewhere [18]. Only an overview of the behavior of the PαMSAN/PMMA blends will be given here. Figure 22 shows the curves of crack growth as a function of the stress intensity factor difference, ΔK, for PαMSAN and PMMA. The crack propagation threshold is higher for PMMA than for PαMSAN. This result is in agreement with the observation that PαMSAN is more brittle than PMMA. The curves for the blends all lie between the curves of the neat components. The ΔK value for the threshold increases linearly with increasing PMMA content (Fig. 23). Tests on the annealed samples of PαMSAN/PMMA 85/15 and 40/60 showed that the differences in morphology did not affect the crack growth resistance significantly. On the other hand, if the fracture surface is investigated by SEM, some differences in the fracture mechanism can be observed.

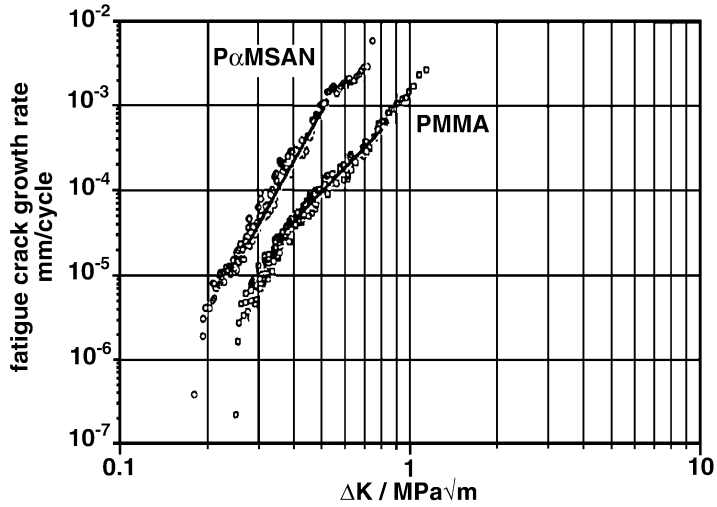

Fig. 22 Fatigue crack growth rate as a function of the stress intensity factor difference, ΔK, for 100 % PαMSAN and 100 % PMMA.

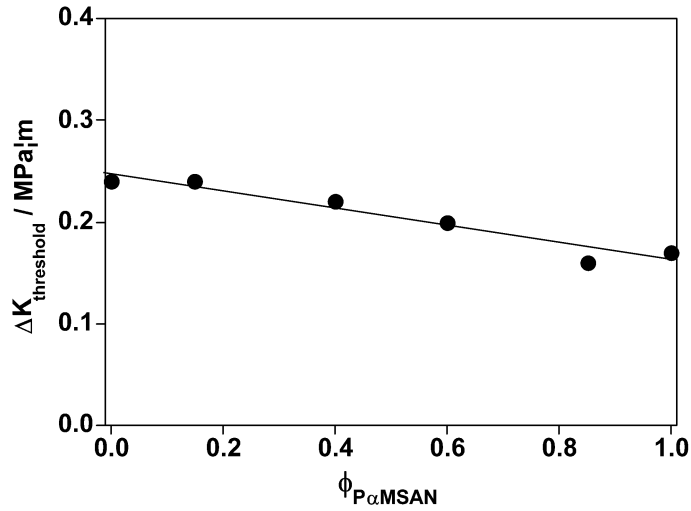

Fig. 23 Stress intensity factor difference, ΔK_{th}, of the blends as a function of the mass fraction of PαMSAN.

The fracture surface of both PαMSAN and PMMA samples show distinct fatigue striations parallel to the direction of crack propagation [16]. Figure 24 shows the fracture surface of a 60/40 blend in the threshold region. For this blend, equally spaced fatigue striations can also be observed, indicating that in this material crack propagation occurred in a discontinuous way, in which the crack advanced in jumps, leaving these distinctive features at regular intervals. In the micrograph, no indication of decohesions or interfacial failures can be seen and apparently both phases are contributing equally to crack propagation.

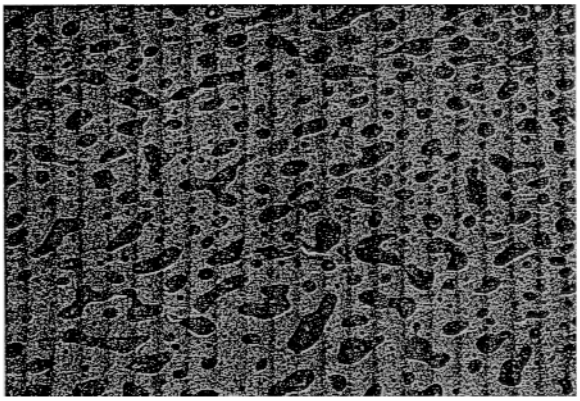

Fig. 24 Scanning electron micrograph showing the threshold region on the fracture surface of the PαMSAN/PMMA 60/40 blend. (Magnification: 1000×.)

In Fig. 25, the fracture surface of the PαMSAN/PMMA 40/60 blend annealed at 220 °C for 4 h is shown. The blend presents a much coarser co-continuous morphology than the unannealed PαMSAN/PMMA 60/40 blend. Also, in this case, fatigue striations on the fracture surface can be observed. A closer observation (Figs. 26 and 27), however, shows that the different phases contributed differently to crack propagation in this sample. Figure 26 shows a region, where the crack enters the PαMSAN phase. At the beginning, the space between striations is approximately 10 μm, similar to that observed for neat PMMA, but as a crack propagates in the PαMSAN phase the distance between striations drops to below 5 μm, as was observed for neat PαMSAN. These observations indicate that as a

Fig. 25 Scanning electron micrograph of the annealed PαMSAN/PMMA 40/60 blend. Crack propagation velocity: 10^{-5} mm/cycle. (Magnification: 130×)

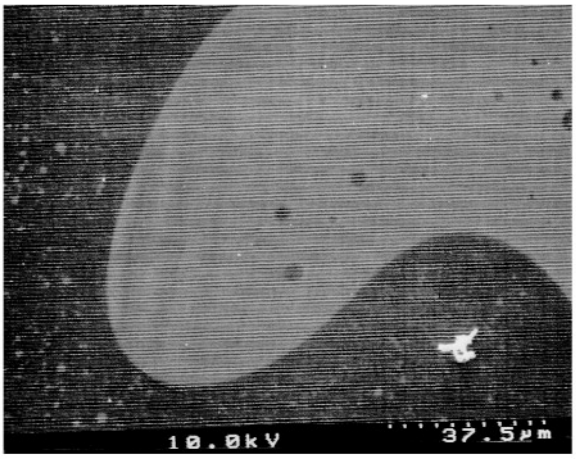

Fig. 26 Scanning electron micrograph of the annealed PαMSAN/PMMA 40/60 blend (same as Fig. 25). Crack propagation velocity: 10^{-5} mm/cycle. (Magnification: 800×)

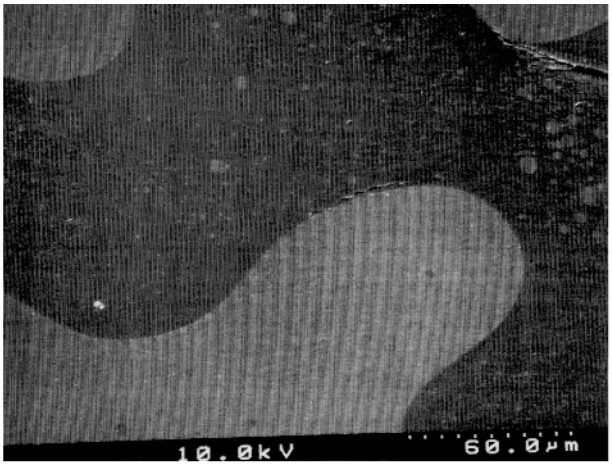

Fig. 27 Scanning electron micrograph of the annealed PαMSAN/PMMA 40/60 blend (same as Fig. 25). Crack propagation velocity: 10^{-5} mm/cycle. (Magnification: 500×)

crack enters the PαMSAN phase, it continues to propagate as it did in the PMMA phase, but as a crack advances inside the phase its growth mechanism becomes more and more influenced by the properties of the phase in which it is growing. In Fig. 27, a region where the crack leaves the PαMSAN phase is shown. The striations appear curved in this region, suggesting a gradient in crack velocity between the two phases. All these observations suggest that the crack propagates faster in the more brittle PαMSAN phase than in the PMMA phase. It is also interesting to note that this gradient in the crack propagation rate resulted in the formation of cracks at or close to the interface between the two polymer phases (Fig. 27).

The investigation of the fracture surfaces shows that, even though in the crack propagation curves no evidence for different mechanisms in the different blends could be observed, for the blends with fine morphologies, the crack propagation appears to be uniform across the crack front, while for blends with coarser morphologies, the crack propagation velocity is determined by the properties of the phase in which the crack is growing.

CONCLUSIONS

A very interesting feature of PαMSAN/PMMA blends is the possibility of strongly influencing the morphology without changing the composition. Alongside the investigation of the effect of blend composition, the influence of morphology on mechanical properties can be investigated only by annealing without changing chemistry. For this, the influence of annealing on the blend morphology has to be understood with the help of a phase diagram. Based on TEM micrographs and cloudpoints of 17 blends with different compositions, the interaction parameters were determined to calculate the spinodal of the LCST system. In accordance with the phase diagram, annealing results in a finer morphology for the 85/15 blend (nearly transparent) while the domain size is significantly increased in the 40/60 blend with annealing time. The glass-transition temperatures from DSC measurements confirm that the blends of all compositions were completely phase-separated. Although significant changes in the morphology could be achieved by annealing, no significant changes in the glass-transition temperatures were observed. The storage modulus from the dynamic mechanical analysis follows a rule of mixture as a function of composition and temperature, in agreement with Young's and flexural modulus from tensile tests. Because PαMSAN and PMMA present very broad α-relaxations, it is very difficult to identify two separated relaxation processes in the dynamic mechanical analysis. Tensile strength and fracture toughness indicate that the PαMSAN domains in the tougher PMMA matrix causes a deterioration in the mechanical properties of the blends, while the PMMA domains in the PαMSAN matrix improved the mechanical properties. No clear conclusions about the influence of morphology on fracture toughness could be drawn because in one case (40/60 blend) the fracture toughness decreases slightly on annealing, whereas in the other case (85/15 blend) fracture toughness increased slightly with decreasing phase separation by annealing. In situ strained thin sections in the TEM indicated no effect of annealing on the micromechanical behavior. Shear deformation was observed as the prevailing deformation mechanism in the PαMSAN and fibrillized crazing in the PMMA-rich blends. From fatigue crack growth experiments, it was concluded that the crack propagation threshold is higher for PMMA than for PαMSAN. The ΔK value for the threshold increases linearly with increasing PMMA content. Tests on the annealed samples of PαMSAN/PMMA 85/15 and 40/60 showed that the differences in morphology did not affect the fatigue crack growth resistance significantly. From the features of the fracture surface investigated by SEM, the conclusion can be drawn that the fatigue crack propagates faster in the more brittle PαMSAN phase, but the overall advance of the crack front is controlled at the interphase, resulting in a crack propagation gradient along the interphase.

REFERENCES

1. H. M. Laun. *Pure Appl. Chem*. **70**, 1547–1566 (1998).
2. V. Schytt and J. Lyngaae-Jørgensen. *Polym. Networks Blends* **7**, 77–86 (1997).
3. I. Vinckier and H. M. Laun. *Rheol. Acta* **28**, 274–286 (1999).
4. I. Vinckier and H. M. Laun. *Macromol. Symp*. 151–156 (2000).
5. Z. I. Zhang, H. D. Zhang, Y. L. Yang, I. Vinckier, H. M. Laun. *Macromolecules* **34** (5), 1416–1429 (2001).
6. D. W. Schubert. *Mater. Res. Innovation* **4**, 353 (2001).
7. S. H. Goh, D. R. Paul, J. W. Barlow. *Polym. Eng. Sci.* **22** (1982).
8. D. R. Paul and C. B. Bucknal. *Polymer Blends*, Vols. 1 and 2, John Wiley, New York (2000).
9. L. A. Utracki. *Polymer Alloys and Blends: Thermodynamics and Rheology*, Hanser, Munich (1987).
10. O. Olabisi, L. M. Robenson, M. T. Shaw. *Polymer-Polymer Miscibility*, Academic Press, New York (1979).
11. R. P. Wool. *Polymer Interfaces: Structure and Strength*, Hanser, Munich (1995).
12. J. L. Willet and R. P. Wool. *Macromolecules* **25**, 5336 (1993).

13. M. E. Fowler, J. W. Barlow, D. R. Paul. *Polymer* **28**, 1177 (1987).
14. ISO/DIS 13586.2 (1998).
15. ISO/DIS 15850 (1999).
16. C. Koster, Diplomarbeit, Ecole Polytechnique Féderale de Lausanne.
17. N. G. McCrum, B. E. Read, G. Williams. *Anelastic and Dielectric Effects in Polymeric Solids*, Dover Publications, New York (1991).
18. C. Koster, V. Altstädt, H. H. Kausch, W. J. Cantwell. *Polym. Bull.* **34**, 243–248 (1995).